1

Introduction

Coriolis Vibratory Gyroscopes (CVGs) are mechanical transducers that detect angular rotation around a particular axis. In its most fundamental form, a CVG consists of two or more mechanically coupled vibratory modes, a forcing system to induce vibratory motion and a sensing system to detect vibratory motion. Angular rotation can be detected by sensing the energy transfer from one vibratory mode to another in the presense of Coriolis forces, Figure 1.1.

Historically, first examples of CVGs can be found in the Aerospace Industry, which were primarily used for navigation and platform stabilization applications. Later, advent of Micro-electromechanical System (MEMS) fabrication techniques brought along orders of magnitude reduction in cost, size, weight, and power (CSWaP), which made CVGs truly ubiquitous. Today CVGs are used in a wide variety of civilian applications, examples include:

- Industrial applications, such as robotics and automation;
- Automobile stabilization, traction control, and roll-over detection;
- Gesture recognition and localization in gaming and mobile devices;
- Optical image stabilization (OIS) of cameras;
- Head tracking in Augmented Reality (AR) and Virtual Reality (VR);
- Autonomous vehicles, such as self-driving cars and Unmanned Aerial Vehicles (UAVs).

1.1 Types of Coriolis Vibratory Gyroscopes

CVGs can be divided into two broad categories based on the gyroscope's mechanical element [1]: degenerate mode (i.e. z-axis) gyroscopes, which have x–y symmetry (Δf of 0 Hz), and nondegenerate mode gyroscopes, which are designed intentionally to be asymmetric in x and y modes ($\Delta f \neq 0$Hz). Degenerate mode z-axis gyroscopes offer a number of unique advantages compared to nondegenerate vibratory rate gyroscopes, including higher rate sensitivity, ability

Whole-Angle MEMS Gyroscopes: Challenges and Opportunities,
First Edition. Doruk Senkal and Andrei M. Shkel.

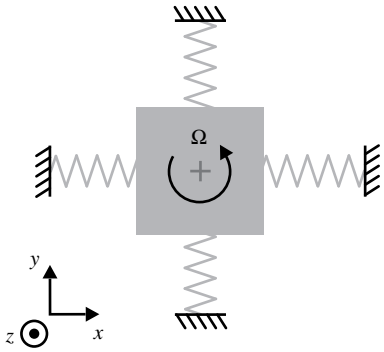

Figure 1.1 Coriolis Vibratory Gyroscopes, in their simplest form, consist of a vibrating element with two or more mechanically coupled vibratory modes. Illustration shows a *z*-axis gyroscope and its vibratory modes along *x*- and *y*-axis.

to implement whole-angle mechanization with mechanically unlimited dynamic range, exceptional scale factor stability, and a potential for self-calibration.

1.1.1 Nondegenerate Mode Gyroscopes

Nondegenerate mode CVGs are currently being used in a variety of commercial applications due to ease of fabrication and lower cost. Most common implementations utilize two to four vibratory modes for sensing angular velocity along one to three axes. This is commonly achieved by forcing a proof mass structure into oscillation in a so-called "drive" mode and sensing the oscillation on one or more "sense" modes. For example, the *x*-axis of the gyroscope in Figure 1.1, can be instrumented as a drive mode and the *y*-axis can be instrumented as a sense mode. When a nonzero angular velocity is exerted (i.e. along the *z*-axis in Figure 1.1), the resultant Coriolis force causes the sense mode (i.e. the mode along the *y*-axis in Figure 1.1) to oscillate at the drive frequency at an amplitude proportional to input angular velocity.

Resonance frequency of sense modes are typically designed to be several hundreds to a few thousand hertzs away from the drive frequency. The existence of this so-called drive-sense separation (Δf) makes nondegenerate mode gyroscopes robust to fabrication imperfections. However, a trade-off between bandwidth and transducer sensitivity exists since smaller drive-sense separation frequency leads to higher transducer sensitivity, while the mechanical bandwidth of the sensor is typically limited by drive-sense separation (Δf).

Nondegenerate mode gyroscopes are typically operated using open-loop mechanization. In open-loop mechanization, "drive" mode oscillation is sustained via a positive feedback loop. The amplitidue of "drive" mode oscillations are controlled via the so-called Amplitude Gain Control (AGC) loop. No feedback loop is employed on the "sense" mode, which leaves "sense" mode proof mass free to oscillate in response to the angular rate input.

1.1.2 Degenerate Mode Gyroscopes

Degenerate mode gyroscopes utilize two symmetric modes for detecting angular rotation. For an ideal degenerate mode gyroscope, these two modes have identical stiffness and damping; for this reason typically an axisymmetric or x–y symmetric structure is used, such as a ring, disk, wineglass, etc. Degenerate mode gyroscopes are commonly employed in two primary modes of instrumentation: (i) force-to-rebalance (FTR) (rate) mechanization and (ii) whole-angle mechanization.

In FTR mechanization, an external force is applied to the vibratory element that is equal and opposite to the Coriolis force being generated. This is a rate measuring gyroscope implementation, where the magnitude of externally applied force can be used to detect angular velocity. The main benefit of this mode of operation is to boost the mechanical bandwidth of the resonator, which would otherwise be limited by the close to zero drive-sense separation (Δf) of the degenerate mode gyroscope.

In the whole-angle mechanization, the two modes of the gyroscope are allowed to freely oscillate and external forcing is only applied to null the effects of imperfections such as damping and asymmetry. In this mode of operation the mechanical element acts as a "mechanical integrator" of angular velocity, resulting in an angle measuring gyroscope, also known as a Rate Integrating Gyroscope (RIG).

Whole-angle gyroscope architectures can be divided into three main categories based on the geometry of the resonator element: (i) lumped mass systems, (ii) ring/disk systems, and (iii) micro-wineglasses. Ring/disk systems are further divided into three categories: (i) rings, (ii) concentric ring systems, and (iii) disks. Whereas, micro-wineglasses are divided into two categories according to fabrication technology: surface micro-machined and bulk micro-machined wineglass gyroscope architectures, Figure 1.2 [2].

String and bar resonators can also be instrumented to be used as whole-angle gyroscopes, even though these types of mechanical elements are typically not used at micro-scale due to limited transduction capacity. In principle, any axisymmetric elastic member can be instrumented to function as a whole-angle gyroscope.

1.2 Generalized CVG Errors

Gyroscopes are susceptible to a variety of error sources caused by a combination of inherent physical processes as well as external disturbances induced by the environment.

Error sources in a single axis rate gyroscope can be generalized according to the following formula:

$$\tilde{\Omega} = (1 + S_e)\Omega + b_g + n_g, \tag{1.1}$$

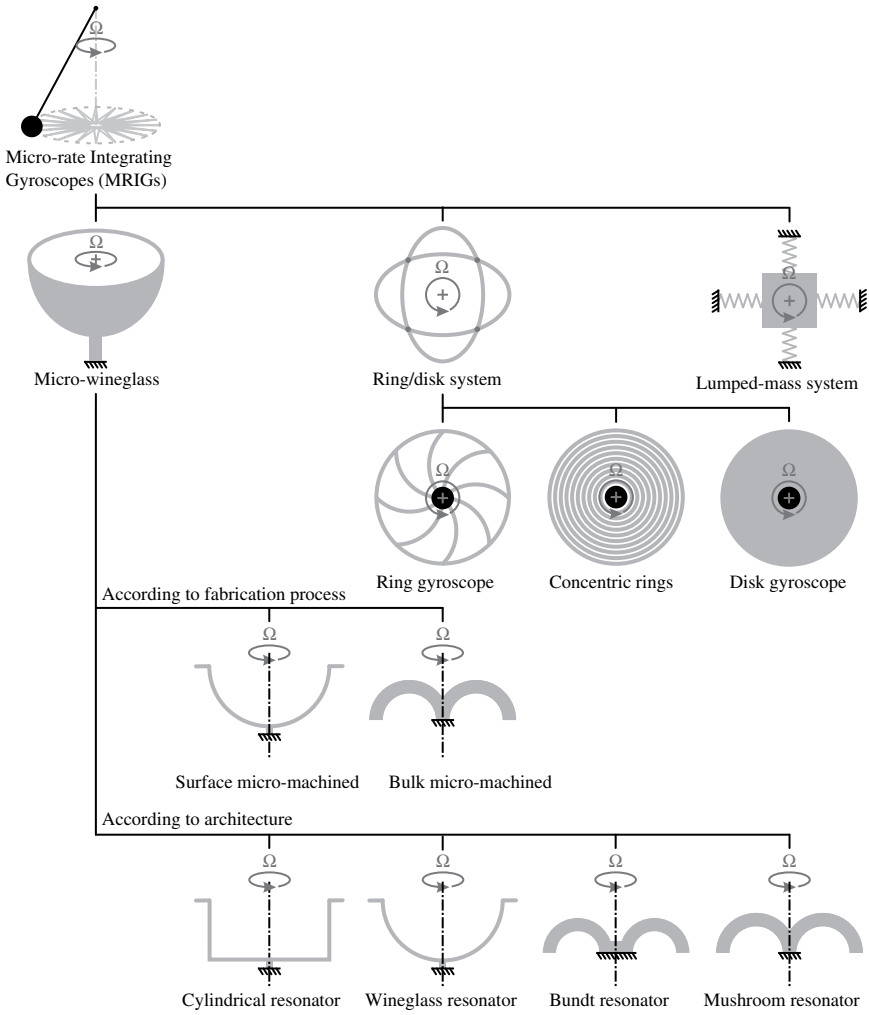

Figure 1.2 Micro-rate integrating gyroscope (MRIG) architectures.

where $\tilde{\Omega}$ is the measured gyroscope output, S_e is scale factor error, b_g is bias error, and n_g is noise. Without loss of generality, for a whole-angle gyroscope the error sources can be written as:

$$\tilde{\theta} = \int ((1 + S_e)\Omega + b_g)\mathrm{d}t + n_g, \tag{1.2}$$

where $\tilde{\theta}$ is the measured gyroscope output, corresponding to total angular read-out, including the actual angle of rotation, errors in scale factor, bias, and noise.

1.2.1 Scale Factor Errors

Scale factor (or sensitivity) errors represent a deviation in gyroscope sensitivity from expected values, which results in a nonunity gain between "true" angular rate and "perceived" angular rate. Scale factor errors can be caused by either an error in initial scale factor calibration or a drift in scale factor postcalibration due to a change in environmental conditions, such as a change in temperature or supply voltages, application of external mechanical stresses to the sensing element, or aging effects internal to the sensor, such as a change in cavity pressure of the vacuum packaged sensing element.

1.2.2 Bias Errors

Bias (or offset) errors can be summarized as the deviation of time averaged gyroscope output from zero when there is no angular rate input to the sensor. Aside from initial calibration errors, bias errors can be caused by a change in environment conditions. Examples include a change in temperature, supply voltages or cavity pressure, aging of materials, and application of external mechanical stresses to the sensing element. An additional source of bias errors is external body loads, such as quasi-static acceleration, as well as vibration.

1.2.3 Noise Processes

Noise in gyroscopes can be grouped under white noise, flicker $(1/f)$ noise, and quantization noise. The most common numerical tool for representing gyroscope noise processes is Allan Variance.

1.2.3.1 Allan Variance

Originally created to analyze frequency stability of clocks and oscillators, Allan Variance analysis is also widely used to represent various noise processes present in inertial sensors, such as gyroscopes [3]. Allan Variance analysis consists of data acquisition of gyroscope output over a period of time at zero rate input and constant temperature. This is followed by binning the data into groups of different integration times:

$$\overline{\Omega}_n(\tau) = \frac{1}{\tau}\int_{n\tau_0}^{n\tau_0+\tau} \Omega(t)\mathrm{d}t, \tag{1.3}$$

where τ_0 is the sampling time, n is the sample number, and $\tau = m\tau_0$ is the bin size. The uncertainty between bins of same integration times is calculated using ensemble average:

$$\sigma^2(\tau) = \frac{1}{2} < (\overline{\Omega}_{n+m}(\tau) - \overline{\Omega}_n(\tau))^2 >. \tag{1.4}$$

Finally, the calculated uncertainty $\sigma(\tau)$ with respect to integration time (τ) is plotted to reveal information about various noise processes within the gyroscope, Figure 1.3. Sections of the Allan Variance curve and their physical meaning is summarized below [3]:

- **Quantization noise** is due to the conversion of gyroscope output from analog (continuous) signal to digital (countable) signal by Analog-to-Digital Converters (quantization). Quantization noise has a slope of τ^{-1} on the Allan variance graph.
- **Angle Random Walk (ARW)** is caused by white thermomechanical and thermoelectrical noise within the gyroscope, shows up with a slope of $\tau^{-1/2}$. It is usually reported using units $^\circ/\sqrt{h}$ (degrees per square root of hour) or mdps/$\sqrt{\text{Hz}}$ (millidegrees per second per square root of hertz).
- **Rate Random Walk (RRW)** is the random drift term within the gyroscope, shows up with a slope of $\tau^{+1/2}$ opposite of ARW.
- **Bias instability** is the lowest point of the Allan variance curve, shows up with a slope of zero. It represents the minimum detectable rate input within the gyroscope and is reported using units $^\circ/h$ (degrees per hour) or mdps (millidegrees per second). Bias instability is limited by a combination of flicker $(1/f)$ noise, ARW, and RRW.

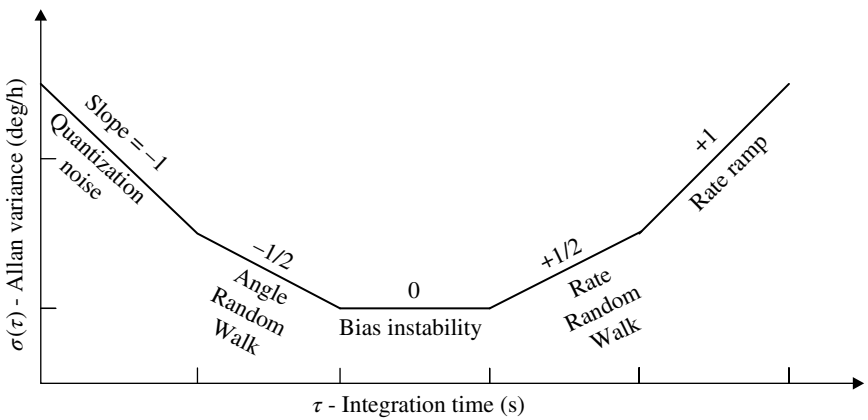

Figure 1.3 Sample Allan variance analysis of gyroscope output, showing error in gyroscope output (deg/h or deg/s)with respect to integration time (s).

- **Rate ramp**, also called the thermal ramp, is caused by temperature changes in the environment, shows up with a slope of τ^{+1}.
- **Periodic oscillations** show up as peaks in the Allan Variance curve with an integration time of 1/frequency (not shown). These oscillations are either caused by a periodic event in sensor electronics or the environment, such as day/night temperature cycles or variations in power supply.

1.3 Overview

The first part of this book focuses on fundamentals of whole-angle gyroscopes, dynamics, mathematical framework, and control strategies. In the second part of the book, conventionally micro-machined 2-D whole-angle gyroscope architectures are reviewed. The final part of the book focuses on 3-D emerging micro-machining technologies for fabrication of whole-angle gyroscope architectures.

In Chapter 2, Foucault Pendulum analogy is introduced as a starting point for whole-angle gyroscope dynamics. Later in the chapter, effects of structural imperfections are introduced, along with requirements for continuous RIG operation.

In Chapter 3, a brief overview of control strategies for CVGs is presented. The remainder of the chapter deals with sustaining oscillation and suppression of error sources in whole-angle gyroscopes, along with methods for tuning and self-calibration.

Chapter 4 provides an overview on two types of conventionally micro-machined 2-D micro-machined whole-angle gyroscope architectures: lumped mass gyroscopes and distributed mass gyroscopes.

In Chapter 5, two examples of 2-D micro-machined whole-angle gyroscope architectures are reviewed: (i) Toroidal Ring Gyroscope (TRG) and (ii) Dual Foucault Pendulum (DFP) gyroscope. The goal of this chapter is to illustrate factors that influence design decisions, fabrication considerations, and characterization methodology.

In Chapter 6, recent advances in 3-D shell micro-technology for fabrication of whole-angle gyroscopes are reviewed. Starting with a brief history of macro-scale shell resonator gyroscopes, the chapter focuses on advances in micro-shell resonator fabrication processes, with an emphasis on transduction mechanisms, characterization techniques, and mechanical properties.

In Chapter 7, the micro-glassblowing paradigm is introduced for wafer-level fabrication of atomically smooth, low internal loss Titania Silicate Glass (TSG) and fused silica 3-D wineglass gyroscopes. Feasibility of the process has been demonstrated by fabrication of fused silica and TSG micro-glassblown structures.

In Chapter 8, various transduction strategies for micro-glassblown wineglass resonators are presented. Two methods of electrostatic transduction are reviewed in this chapter: (i) in-plane electrodes and (ii) out-of-plane electrodes.

Finally, the book is concluded in Chapter 9 with an outlook of future trends.